Sedimentation from particle-bearing plumes in a stratified ambient

Bruce R. Sutherland[1,2,*] and Youn Sub (Dominic) Hong[3]

[1]*Department of Physics, University of Alberta, Edmonton, Alberta T6G 2E1, Canada*
[2]*Department of Earth and Atmospheric Sciences, University of Alberta, Edmonton, Alberta T6G 2E3, Canada*
[3]*Department of Engineering Science, University of Toronto, Toronto, Ontario M5S 1A1, Canada*

Laboratory experiments are performed to examine the sedimentation of particles that initially rise in a plume, then spread radially and settle in uniformly stratified fluid. Using light attenuation, the depth of the sediment bed is measured nonintrusively as a function of radius from the center of the plume. To gain some insight into these dynamics, an idealized model is developed by adapting well-established plume theory and a theory that accounts for sedimentation from surface gravity currents emanating from a plume impacting a rigid lid. We also account for recycling of falling particles that are re-entrained into the plume. With a suitable choice of parameters determining the intrusion height, entrainment during fountain collapse, and the radius at which settling from the intrusion begins, in most cases for which particles are predicted to be drawn back into the plume and recycled. The predictions for intrusion height, particle mound height, and spread agree within 20% of observations.

I. INTRODUCTION

The study of particle-bearing plumes in stratified fluid provides a starting point to understand the spread of ash from large volcanic eruptions that penetrate into the stratosphere [1]. Over several decades, theories have been developed to gain insight into the three components of the system: the plume rise [2–5], the radial spread of the intrusion [6–8], and the sedimentation and possible re-entrainment of particles into the plume [9,10]. Much of this work has been tested against observations from laboratory experiments. Experiments with non-particle-bearing plumes have been used to test predictions of plume rise, collapse, and spread [11–14]. Experiments with particle-bearing plumes are much more challenging to perform and analyze [9,10,15,16], not least because of the challenge in establishing a constant particle flux and in measuring the depth of sediment that builds up as particles settle to the ground. Often this is done in a time-consuming way through direct measurement, successively extracting samples and measuring the contained mass of particles. The work presented here will use a recently developed light-attenuation technique [17–19] to measure nonintrusively the depth versus radius of sediment resulting from particles settling from a particle-bearing plume rising and spreading axisymmetrically in a uniformly stratified fluid. The results are compared with a model that combines and adapts several of the theories for plume rise and spread and particle settling.

It is impossible directly to measure in the field the source conditions of an exploding volcano. Instead, they are inferred from indirect measurements. The most common of these measure the maximum rise of the Plinian column [20] and from the lateral spread of ash from the column in what is called an umbrella cloud. Another way indirectly to assess the source conditions is to measure the distribution of ash that has settled on the ground around the volcano after the main eruption. But it is nontrivial to make the connection between the lateral profile of sediment depth with the evolution of particles from source to umbrella cloud to settling.

Early experiments on particle-bearing plumes in uniform-density ambients focused upon their qualitative dynamics as they were influenced primarily by particle concentration [15]. Digital

---

*bruce.sutherland@ualberta.ca; [https://www.ualberta.ca/∼bsuther](https://www.ualberta.ca/~bsuther)
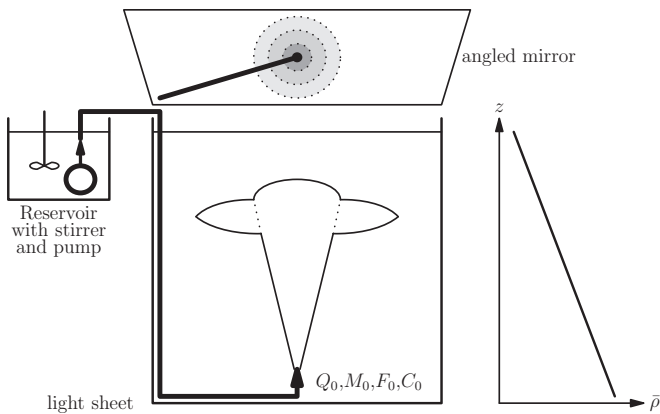
FIG. 1. Schematic of the experiment setup showing a cubical tank filled with uniformly stratified fluid with reservoir to the upper left. A pump drives particle-bearing fluid from the reservoir through a hose passing down the rear-left corner of the tank and diagonally along the bottom to a nozzle pointing upward in the middle of the tank. An angled mirror above the tank is used to measure the deposition of particles by recording the attenuation of light from a light sheet placed at the bottom of the tank.

recording methods were later used to measure the radius and spread of such plumes [10]. Using the setup of Carey *et al.* [15], the settled particle concentration was measured as a function of radial distance through careful extraction and weighing of samples of the sediment bed at the end of an experiment [6,9]. This research found that the theory predicting the mass of settled particles underpredicted the observed values, particularly in cases for which the buoyancy flux was large and significant particle re-entrainment occurred.

Few experiments have examined particle-bearing flows in stratified fluid. Holasek *et al.* [21] performed experiments studying the spread of a particle-bearing intrusion in stratified fluid in order to examine the separation of interstitial fluid gas from the settling particles in an umbrella cloud. The experiments by Carazzo and Jellinek [22,23] examined both the rise and spread of a particle-bearing plume in uniformly stratified fluid. Their analysis focused upon structure and stability of the plume, whether it was stable (forming an umbrella cloud-like intrusion) or unstable (collapsing all or in part to form a bottom-propagating particle-laden gravity current). Mirajkar *et al.* [16] also examined the rise and spread of a particle-bearing plumes in uniformly stratified fluid, focusing upon the influence of particle concentration upon rise height and the radial spread of the intrusion. In none of these studies was the mass distribution of settled particles measured.

This work begins in Sec. II with a description of the experiment setup and analytical methods. Therein measurements of the height of the spreading intrusion are presented by analogy to measurements of particle-free plumes and fountains in stratified fluid [12,14]. The measured particle mound height and radius are tabulated and discussed. In Sec. III, the combined theory for plume rise and spread and for particle settling and recycling is described. The comparison between this theoretical model and experiment results is discussed in Sec. IV, and conclusions are given in Sec. V.

II. EXPERIMENT SETUP AND ANALYSIS METHODS

The experimental setup is shown in Fig. 1. Experiments were performed in a open-lidded cubical tank measuring 50 cm on each side. Beneath the initially empty tank was placed a fluorescent light sheet (Electric Vinyl Inc.) and on top of the tank was placed a mirror angled at 45°. A nozzle with circular opening of radius 0.28 cm was positioned at the center of the tank pointing vertically upward. Crossed wires were fastened just below the opening of the nozzle in order to trip turbulence. The opening of the nozzle itself was $z_0 = 5.7$ cm above the tank bottom. In some experiments, a

10-cm-tall vertical barrier running parallel to the right tank wall was positioned 5 cm to the right of the nozzle. The region between the barrier and tank wall was used to calibrate the relationship between the amount of light passing through a bed of particles and the particle depth, as described in detail below. The barrier itself helped prevent contamination of the calibration by particles spreading and settling from the plume. Repeat experiments showed the presence or absence of the barrier did not significantly affect the results.

A reservoir was filled with a volume V_r of (usually fresh, but sometimes saline) water of density ρ_r. To this was added a mass M_{pr} of approximately spherical glass particles (ballotini, Manus Abrasive Systems Inc.) of mean radius r_p and density $\rho_p = 2.4$ g/cm^3. Different sized particles were used, but good measurements were made only for experiments having particles with mean diameter $100\,\mu$m ($74\,\mu$m $< d_p < 125\,\mu$m) and $214\,\mu$m ($177\,\mu$m $< d_p < 250\,\mu$m). Smaller particles were carried to the tank side walls before settling significantly; larger particles rained down significantly within the column of the plume. The particle concentrations ranged from $C_0 = 0.005$ to 0.037 g/cm^3 (volume fractions of 0.2% to 1.5%), corresponding to mean interparticle separations greater than 6 particle radii at the source. Because the separation distance widens as the particles rise in the expanding plume, particle-particle interactions were not expected to play an important role in the dynamics.

A small amount of fluorescene dye was added to the reservoir, ultimately allowing us to track the advance of injected fluid. While stirring the reservoir to keep the particles in suspension, a centrifugal pump in the reservoir was turned on so that the fluid-particle mixture was forced along a hose down one corner of the empty tank, along the bottom and up through a nozzle in the tank center. When the mixture began to pour out of the nozzle, the pump was turned off and any fluid and particles that had poured out of the nozzle were removed from the tank.

With the reservoir, hose, and nozzle thus primed, the tank was filled to a depth $H_t \simeq 40$ cm with salt-stratified fluid using the double-bucket method [24]. After filling, samples were extracted at 5-cm depth intervals and their density was measured using a densitometer (Anton Paar DMA4500). A plot of density versus depth confirmed that the ambient fluid was uniformly stratified and a best-fit line through the data was used to determine the density gradient and hence the buoyancy frequency.

A digital camera (Canon Rebel T3i) was placed approximately 3 m to one side of the tank with lens at a height moderately below the surface of the ambient fluid in the tank. The field of view simultaneously included the side view of the tank and the top view by way of the angled mirror.

At the start of an experiment, the reservoir was stirred up again and, while continuing to stir, the centrifugal pump was turned on. Immediately in the tank, this fluid-particle mixture was observed to rise vertically from the nozzle, mixing turbulently with the stratified ambient. The typical Reynolds number of the flow at the source was 2000, based upon the mean vertical velocity and the radius of the nozzle opening.

Top- and side-view images taken from a typical experiment are shown in Fig. 2. Although particles initially in the hose had settled while the tank was being filled with ambient fluid, we found that they immediately resuspended after the pump was turned back on. After a few seconds, the flow emanating from the nozzle appeared to be in quasisteady state, with little variation of particle concentration and with uniform flow rate, as observed from the near-constant height of the fountain over time.

In most experiments the pump was turned on and the reservoir stirred for 90 s, and then the pump was turned off. While the pump was running, the particle-bearing fluid from the nozzle was observed to rise while mixing with the ambient, reached a maximum height, fell back upon itself as a fountain, and then spread radially as an intrusion. Except in a few experiments with high particle concentrations, the maximum fountain height and the spreading height of the intrusion were approximately constant. In particular, averaging over short-time fluctuations, the maximum height varied by less than a centimeter over the duration of most experiments. The side view of the experiment clearly showed the advance of the injected fluid through the presence of fluorescene-dyed fluid. In particular, we used the mean vertical height of the fluorescene-dyed fluid in the tank at the end of an experiment as a measure of the intrusion height. This was measured directly by the experimenter, not from the camera images, which sometimes viewed the intrusion from a top-down perspective.
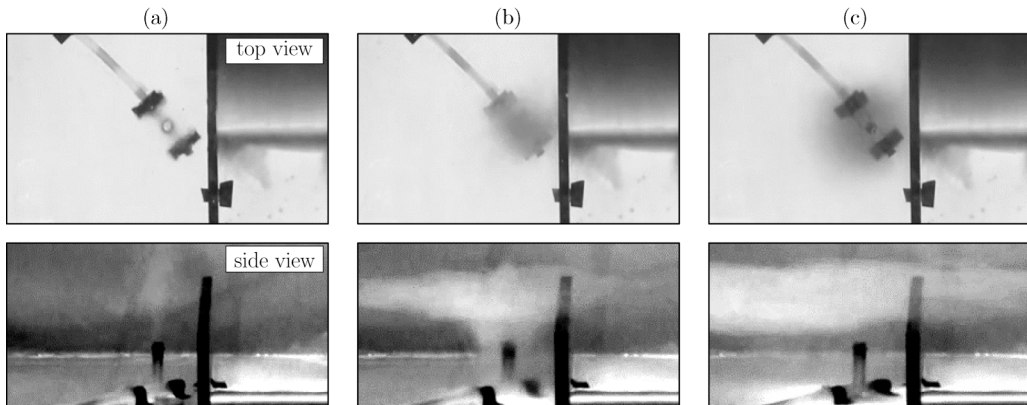
FIG. 2. (Multimedia online) Snapshots taken from experiment 2 (see Table I) taken at times (a) 5 s, (b) 30 s, and (c) 105 s after its start when flow through the nozzle begins. The flow is stopped after 90 s.

In experiments with large particle radii and/or concentration, we observed the fountain to collapse quasiperiodically upon itself as particles raining down within the plume significantly slowed its upward momentum. The particle mixture then ran horizontally along the bottom and was observed to rise again. This behavior was described as that of a "low collapsing fountain" by Carey *et al.* [15]. Such complex dynamics are not captured by the theory in Sec. III, and so are not examined in detail here.

Most of our experiments were performed with relatively low particle concentrations and sedimentation was observed to descend from dilute gravity flows from the plume edge and from the spreading intrusion [15].

After the pump was turned off, the experiment continued to be recorded until the particles within the ambient had all settled to the bottom of the tank. From the top-view image of the experiment at this final time we were able to measure the depth of the sediment surrounding the nozzle.

A. Experimental parameters

The evolution of the system was determined by the ambient stratification, the plume source conditions, and the particle concentration and size. Explicitly, the stratification was characterized by the buoyancy frequency $N = [-(g/\rho_{00})d\bar{\rho}/dz]^{1/2}$, in which g is gravity, ρ_{00} is a characteristic density (taken to be that of the ambient at the level of the nozzle), and $\bar{\rho}(z)$ is the ambient density profile with height, z. The plume source is characterized by the source volume flux (Q_0), momentum flux (M_0), and buoyancy flux (F_0). The source volume flux was measured directly from the change of volume in the reservoir over the 90 s of the experiment. From this we calculated the mean vertical velocity at the source $w_0 = Q_0/(\pi b_0^2)$, in which b_0 is the radius of the nozzle. Hence the momentum flux at the source is $M_0 = \pi b_0^2 w_0^2$. The buoyancy flux at the source is $F_0 = \pi b_0^2 w_0 g_0'$, in which $g_0' = g(\rho_0 - \rho_{00})/\rho_{00}$ is the reduced gravity and ρ_0 is the density of the plume fluid at the source determined from the density of the fluid in the reservoir and the particle concentration, C_0.

The particle size was important as it determined the settling speed, w_s. This was measured directly. For particles with diameters $\simeq 100\,\mu$m, the result was comparable to the predicted Stokes settling speed of 0.73 ± 0.02 cm/s, with errors indicating the different salinities near the plume source, depending upon the strength of the ambient stratification. The particles with mean diameter $214\,\mu$m had settling speed approximately 0.75 of the Stokes settling speed of 3.35 ± 0.1 cm/s, consistent with other measurements [19].

Although 27 experiments were performed, many of these were discarded from analysis for various reasons: (i) the particle concentration was too high, resulting in nonuniform flux of particles from the source; (ii) the particle size was too small, so that they spread within the intrusion to the side

TABLE I. Experiment input parameters with typical errors: ambient buoyancy frequency, N ($\pm 0.01\,\mathrm{s}^{-1}$); source volume flux, Q_0 ($\pm 0.1\,\mathrm{cm}^3/\mathrm{s}$); source momentum flux M_0 ($\pm 10\,\mathrm{cm}^4/\mathrm{s}^2$); source buoyancy flux F_0 ($\pm 1\,\mathrm{cm}^4/\mathrm{s}^3$); particle concentration, C_0 ($\pm 0.0005\,\mathrm{g}/\mathrm{cm}^3$); particle settling velocity, w_s ($\pm 0.01\,\mathrm{cm}/\mathrm{s}$). Experimentally measured quantities: intrusion height, z_i ($\pm 2\,\mathrm{cm}$); maximum settled particle mound height, h_s (in cm with indicated errors); particle mound standard deviation, σ_s (in cm with indicated errors). The error in h_s is estimated from the error in the measurements of h at $r = 1\,\mathrm{cm}$. The error in σ_s is given by the error in computing the best-fit Gaussian to measured curves of height as a function of radius, $h(r)$. (The error in h_s from this best-fit procedure is typically an order of magnitude smaller than the error in determining $h(r = 1\,\mathrm{cm})$.) Theoretically modelled quantities: intrusion height, $z_i^\star$; particle mound height, $h_s^\star$; particle mound standard deviation, $\sigma_s^\star$; radius where the mound height is $h_s^\star$, $r_{\min}$.

Expt.	N	Q_0	M_0	F_0	C_0	w_s	z_i	h_s	σ_s	$z_i^\star$	$h_s^\star$	$\sigma_s^\star$	$r_{\min}$
1	0.58	26.8	2920	−160	0.0369	0.75	17	0.373 (±0.019)	3.59 (±0.05)	14.9	0.513	5.82	0.29
2	1.34	17.2	1234	−133	0.0295	0.72	9	0.358 (±0.018)	3.27 (±0.03)	8.2	0.56	3.7	0.29
3	0.47	14.7	883	−99	0.0295	0.76	16	0.282 (±0.017)	2.53 (±0.03)	14.2	0.37	2.6	0.29
4	0.52	14.3	830	−73	0.0295	0.76	17	0.394 (±0.018)	3.32 (±0.11)	13.7	0.38	2.6	0.29
5	1.85	23.2	2193	218	0.0284	0.67	10	0.299 (±0.009)	4.69 (±0.07)	9.6	0.35	5.5	0.29
6	1.40	23.2	2193	75	0.0199	0.72	10	0.258 (±0.011)	3.17 (±0.06)	10.9	0.27	5.3	0.29
7	0.77	20.1	1642	244	0.0199	0.75	16	0.305 (±0.017)	3.23 (±0.05)	16.1	0.17	6.4	0.29
8	1.34	17.9	1298	282	0.0101	0.71	9	0.096 (±0.013)	1.72 (±0.02)	11.0	0.11	5.1	0.29
9	1.42	22.3	2028	381	0.0050	0.71	11	0.069 (±0.006)	2.61 (±0.07)	12.0	0.05	6.1	0.29
10	0.75	19.2	1500	84	0.0295	2.6	15	0.508 (±0.02)	2.41 (±0.03)	15.2	0.89	0.93	7.3
11	0.72	21.0	1792	213	0.0199	2.6	17	0.69 (±0.02)	2.41 (±0.07)	17.3	0.44	1.17	8.5

of the tank and the settled sediment depth was too small to detect; and (iii) the nozzle was not perfectly vertical, resulting in nonaxisymmetric flows and particle settling. In some experiments we were able to measure the approximate axisymmetric spread of the intrusion, but the sediment bed was not axisymmetric or was too shallow to be detectable above errors. The eleven experiments for which sediment depth was axisymmetric and well measured above noise have parameters listed in Table I. The first nine listed had particles with mean diameter $d_p = 100\,\mu\mathrm{m}$ and the last two had $d_p = 214\,\mu\mathrm{m}$. Within each group, the experiments are ordered by decreasing particle concentration and then by increasing source buoyancy flux. Generally, with smaller particle concentration, the source buoyancy flux was larger, though the flux was also influenced by the ambient stratification and, in particular, by the ambient density at the level of the nozzle.

B. Intrusion height

The height of the intrusion is of particular interest to volcanologists because it serves as an indirect measure of the source conditions. Based upon dimensional arguments, the intrusion height for a plume dominated by the buoyancy flux at the source is expected to scale as [25] $Z_i \propto (|F_0|/N^3)^{1/4}$. For a momentum-dominated source, it is expected to scale as [12,14] $Z_i \propto (M_0/N^2)^{1/4}$.

To combine these limits, it is convenient to define the length scale $H_p = (M_0^3/F_0^2)^{1/4}$, which represents the distance from the source where buoyancy begins to dominate over momentum. We also characterize the influence of stratification by the nondimensional quantity [4,12,26]

$$\sigma = \frac{M_0^2 N^2}{F_0^2}, \tag{1}$$

whose square root measures the ratio of the time for a forced plume to rise a distance H_p to the buoyancy period. So the intrusion height relative to H_p is expected to be a function of σ.
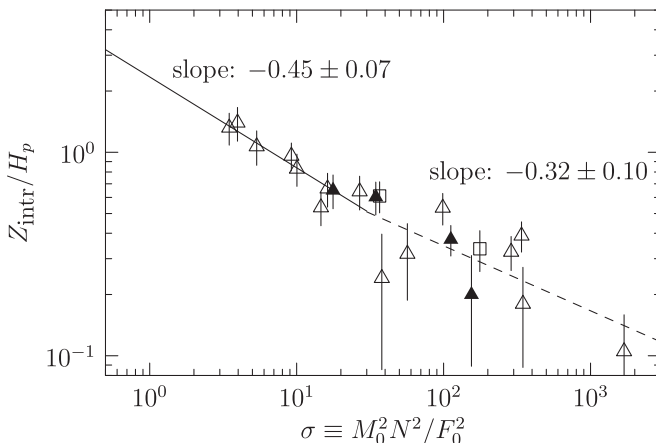
FIG. 3. Relative intrusion height, z_i/H_p, plotted against the relative stratification parameter σ, given by (1). Vertical lines through the points indicate the measurement error, taken to be ± 2 cm. The solid line shows the best fit through data for $\sigma < 30$ and the dashed line shows the best fit through data for $\sigma > 30$. The slope of these lines are indicated above the respective ranges of σ. Symbols correspond to experiments with $F_0 > 0$, $d_p = 100\,\mu$m (open triangles), $F_0 > 0$, $d_p = 214\,\mu$m (open squares), and $F_0 < 0$, $d_p = 100\,\mu$m (closed triangles).

Recent experiments of particle-free plumes in stratified fluid found the following relationship [14]:

$$\frac{Z_i}{H_p} = \begin{cases} 2.73\sigma^{-0.37}, & \text{for } \sigma \lesssim 50 \\ 1.45\sigma^{-0.25}, & \text{for } \sigma \gtrsim 50 \end{cases}. \tag{2}$$

The value for large σ is consistent with that found by Bloomfield and Kerr [12] in their experiments of fountains in stratified fluid (for which $F_0 < 0$).

The intrusion heights measured in our experiments of particle-bearing plumes in stratified fluid are shown in Fig. 3. These include those experiments listed in Table I and others for which measurements of the particle mound height and extent had large errors due to nonvertical (hence nonaxisymmetric) plume rise, but for which measurements of intrusion height varied little in time.

The best-fit lines through the data on a log-log plot give the following relationships:

$$\frac{Z_i}{H_p} = \begin{cases} (2.3 \pm 0.4)\,\sigma^{-0.45\,(\pm 0.07)}, & \text{for } \sigma \lesssim 30 \\ (1.5 \pm 0.8)\,\sigma^{-0.32\,(\pm 0.10)}, & \text{for } \sigma \gtrsim 30 \end{cases}. \tag{3}$$

Consistent with theory [26], other experiments [12,14], and, in particular, the values given in Eq. (2), plumes with large σ intrude at heights that vary with σ approximately as a $-1/4$ power to within the error of measurement. The scatter of points for $\sigma > 30$ can be attributed in part to the relatively large particle concentrations (between 7% and 1.5% by volume) for these experiments. The magnitude of the power-law exponent for plumes with small σ is somewhat larger in magnitude than the predicted value of $-3/8$, though this value is not too far below the lower range of the uncertainty. The results are also consistent with the experiments of Mirajkar *et al.* [16], who showed that while particles within a plume rising in uniformly stratified fluid affect the maximum fountain height, the intrusion spreading height remains constant if the volume concentration of particles is less than 0.5%. It is encouraging that the predictions for non-particle-bearing plumes agree reasonably well with observations. Thus, in our experiments the particles may be assumed to play an effectively passive role during the plume evolution, contributing to the buoyancy flux but not significantly influencing the rise and spread through particle settling within the plume itself.
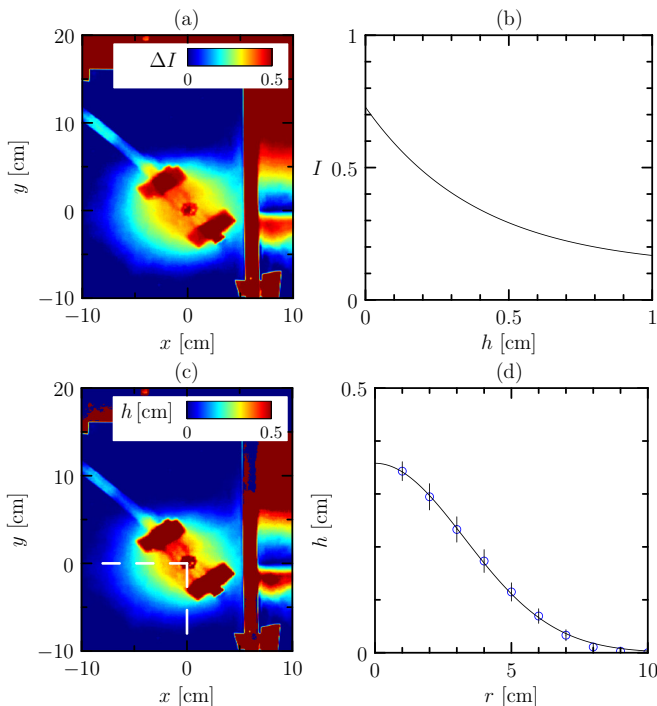
FIG. 4. (a) Top view constructed at the end of experiment 2 (see Table I) showing the measured intensity change $\Delta I = I_0 - I(x,y)$. The two thick, diagonal, dark red strips to the upper left and lower right of the nozzle are a result of electrical tape used to fix the nozzle to the bottom of the tank. (b) Calibration curve (4) with $I_0 = 0.609$, $I_b = 0.119$, and $\sigma_{hI} = 0.396$. (c) Corresponding sediment depth, $h(x,y)$. (d) Corresponding depth as a function of radius $h(r)$ (circles) with errors (vertical lines through circles) found by examining data within the $90°$ sector indicated by the white dashed lines in panel (c). The solid curve plots the best-fit Gaussian through the measured points with maximum $h_0 = 0.358(\pm 0.004)$ cm and standard deviation $\sigma_h = 3.27(\pm 0.03)$ cm.

C. Sediment depth measurement

The sediment depth was measured nonintrusively using light attenuation [17,19]. As with light attenuating when passing through dyed fluid, so does light attenuate when passing through a bed of glass ballotini. The relationship between intensity, I, of light passing through the bed to its depth, h, is

$$I = I_b + (I_0 - I_b)e^{-h/\sigma_{hI}}, \tag{4}$$

in which I_0 is the measured light intensity in the absence of particles, I_b is the measured ("black") light intensity when the particle bed is so thick that no light passes directly through the bed, and σ_{hI} is the measured e-folding depth.

The fluorescent light sheet was found to produce an approximately uniform light intensity (I_0 constant) over the horizontal area of the tank. To determine the values of I_b and σ_{hI}, particles settled at the bottom of the tank were scraped into a wedge-shaped bed whose depth varied linearly with distance from one of the tank walls. The intensity of light passing through this bedform was measured and related to the known depth on a log-linear plot. Best-fit lines through the plot gave the values of I_b and σ_{hI}. The resulting relationship is plotted in Fig. 4(b).

In some cases this calibration procedure was done before and after the experiment by creating the wedge-shaped bedform to one side of a vertical barrier in the tank before it was filled. These
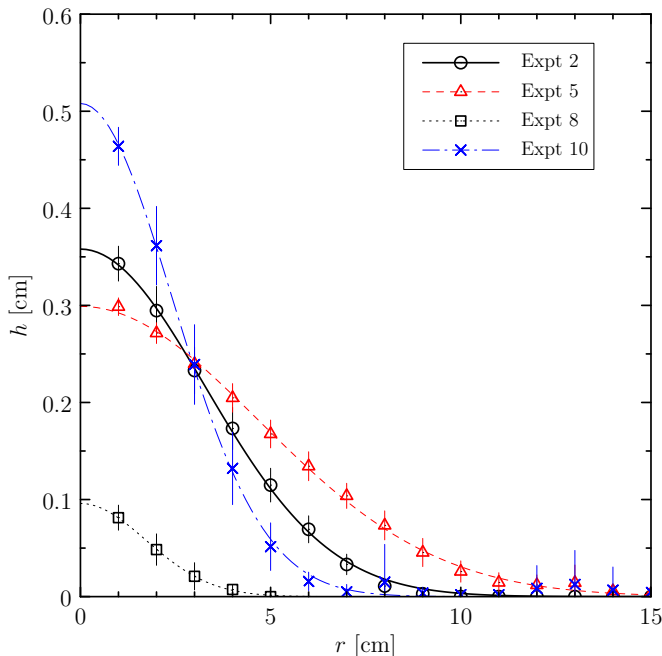
FIG. 5. Measured sediment depth as a function of radius (points with vertical error bars indicated) and the best-fit Gaussian to these points (lines) plotted for four experiments, as indicated in the legend at the upper-right corner of the plot. The values for experiment 2 shown in Fig. 4(d) are replotted here as the circles fit by a solid black curve. The other three experiments are chosen to compare the sediment depth profile in experiment 2 with those measured in experiments having larger buoyancy and momentum flux (experiment 5), smaller particle concentration (experiment 8), and larger particle size (experiment 10).

tests confirmed that the presence of fluorescent dye injected into the tank during the experiment did not affect the results.

From a top-view snapshot taken at the end of an experiment, the intensity of light as a function of horizontal position was measured. This is shown, for example, in Fig. 4(a).

Inverting (4) and using the empirical constants from the calibration plot, the depth of the sediment deposit $h(x,y)$ was found, as shown in Fig. 4(c). For this particular experiment, a 10-cm-tall vertical barrier separated the wedge-shaped bedform used for calibration (outside to the right of this image) and the nozzle region. As a consequence, we found that particle deposition near the wall was inhibited. However, repeat experiments performed with no wall present showed that the deposition pattern on the opposite side of the nozzle was unaffected by the presence of the wall.

In order to measure the depth of deposit as a function of radius, we binned the $h(x,y)$ data into concentric annuli of width 1 cm, and averaged the binned values over the annulus but only within the lower-left sector (where $x,y < 0$). The mean values gave $h(r)$ with a radial resolution of 1 cm. The standard deviation gave the error in the measurement and also provided a check on the assumption of axisymmetry. A typical result, shown in Fig. 4(d), indicates that a Gaussian curve fits very well through the data. The errors of the best-fit values of h_s and σ_s are typically less than 3% of their respective values.

The ninth and tenth columns of Table I list the values of the maximum height and standard deviation of the settled particles measured in eleven different experiments. Figure 5 plots $h(r)$ for a subset of experiments in order to provide a visual comparison for the effect of buoyancy flux, particle concentration, and particle size upon the maximum depth and extent of the sediment mound. As expected, the height of the mound was generally smaller if the particle concentration was smaller.

In the two large-diameter-particle experiments the mound heights are larger and have smaller radial extent than comparable experiments with smaller particle diameters. Other trends are less apparent, which we take as an indication of the variety of processes involved as particles rise and spread from the plume in background stratification and ultimately settle, interacting with the plume as they fall. These dynamics are examined more thoroughly in the next section.

III. THEORY

Here we predict the depth of sediment deposits on the ground resulting from a particle-bearing plume in stratified fluid rising and then spreading laterally in a stratified ambient. Although other modeling studies have considered the effect of horizontal flows, hindered settling, particle aggregation, and polydisperse flows [27–30], our model is restricted to the examination of the experimental conditions in which the ambient is stationary, particle concentrations are relatively small, and nonaggregating particles with a narrow range of particle sizes are used.

The problem is split into three parts. In the first we use the approach of Morton *et al.* [2] to estimate the volume flux and particle concentration of the plume where it spreads at its neutral buoyancy level. Second, we follow the approach of Carey *et al.* [6,15] to estimate the fallout of particles from the radially spreading intrusion. Third, we consider the influence of the z-dependent radial inflow toward the plume to track the path of the particles as they fall toward the ground [9,10]. In some circumstances a fraction of the particles can be re-entrained into the plume, which consequently affects the evolution of the plume, intrusion, and particle settling. An iterative procedure is used to account for such particle recycling [10].

A. Plumes in a stratified ambient fluid

For a Boussinesq plume in statistically steady state, after averaging over long time scales compared to the eddy turnover time, the mean fluxes of specific volume, momentum, and buoyancy as a function of height are given respectively by [2]

$$Q = 2\pi \int wr \, dr = \pi b^2 \bar{w},$$

$$M = 2\pi \int w^2 r \, dr = \pi b^2 \bar{w}^2, \tag{5}$$

$$F = 2\pi \int g'wr \, dr = \pi b^2 \bar{g'} \bar{w},$$

in which r is the radius from the center of the plume, $w(r,z)$ is the time-averaged vertical velocity, and $g'(r,z) = g[\rho(r,z) - \rho_a(z)]/\rho_{00}$ is the reduced gravity expressed as the difference of the plume density (ρ) and ambient density (ρ_a) normalized by the characteristic density (ρ_0, constant). The integrals are conveniently re-expressed in terms of the effective mean radius, $b(z)$, and the horizontally averaged vertical speed, $\bar{w}(z)$, and reduced gravity, $\bar{g'}$.

From the laws of conservation of mass, momentum, and buoyancy, the following coupled differential equations determine the fluxes vary with height z from the source of a rising turbulent plume [2]:

$$\frac{dQ}{dz} = 2\alpha(\pi M)^{1/2}, \tag{6}$$

$$\frac{dM}{dz} = \frac{FQ}{M}, \tag{7}$$

$$\frac{dF}{dz} = -N^2 Q, \tag{8}$$

in which $N^2 = -(g/\rho_{00})d\rho_a/dz$ is the squared buoyancy frequency represented in the Boussinesq approximation and α, the entrainment parameter, is the assumed constant ratio between radial velocity, u_e, of fluid being drawn into the plume at $r = b$ and the mean vertical velocity, $\bar{w}$, at that height. Previous experiments of forced plumes have estimated values of α between 0.06 and 0.17 for so-called top-hat flows, with lower values for jets and higher values in pure plumes (e.g., see the review by Carazzo *et al.* [31]). It has been suggested that α should itself vary as the forced plume advances from the source in a stratified fluid [31,32]. However, given the number range of empirical parameters in the problem being considered here, we chose to fix α at a typical constant value of 0.1.

Analytic similarity solutions can be found in the case of a plume rising in a uniform-density ambient ($N^2 = 0$). But the numerical integration of (6)–(8) is necessary if the ambient is stratified. In such a calculation, the volume, momentum, and buoyancy fluxes (respectively Q_0, M_0, and F_0) are specified at the source, and (6)–(8) are integrated to determine $Q(z)$, $M(z)$, and $F(z)$.

The evolution is more complicated after the plume transforms itself into a fountain when its momentum carries it past its level, z_n, of neutral buoyancy and the buoyancy flux opposes the momentum flux. Thereafter the fluid, after reaching a maximum height, collapses back upon itself and then spreads radially as an intrusion at height z_i. This height is moderately above z_n because entrainment during the rise and fall above this height dilutes the plume fluid further [3,4,12]. While Bloomfield and Kerr [4] attempted to capture some of these effects by adapting plume theory to account for entrainment and detrainment from the downflow about the plume, their model introduced several new parameters to account for the entrainment-detrainment processes and the dynamics at the fountain top. Here we take a different approach, introducing empirical parameters that can be estimated in part by visual observation of the plume dynamics.

In uniformly stratified fluid, empirical predictions for the intrusion height [14] are given by (2). Our experiments show that the presence of particles does not change this prediction significantly, suggesting that particles influence the buoyancy, but settling does not influence the plume dynamics, at least for the particle sizes and most of the particle concentrations we report upon here. For simplicity, we suppose the intrusion height occurs at a fixed fraction of the distance between the maximum height Z_{max} (where $M = 0$) and the neutral height Z_{neutral} (where $F = 0$, or at $z = 0$ if $F < 0$ at the source) so that

$$z_i = Z_{\text{neutral}} + \gamma_z(Z_{\text{max}} - Z_{\text{neutral}}). \tag{9}$$

The value of γ_z should be a number moderately less than unity.

To predict particle concentration in the plume, we suppose that the particle settling velocity is small compared to the plume velocity over most of its width up to the height where the intrusion forms. This is supported by predictions of the model which show that only above the intrusion depth does the settling velocity of particles used in our experiments become comparable in magnitude to the vertical velocity of the plume. Thus we passively advect the concentration field while also accounting for entrainment into the plume of particles settling in the surrounding ambient. Explicitly, the mean particle mass concentration (mass of particles per volume of mixture) is given by assuming the vertical mass-flux of particles in the plume changes only due to lateral entrainment below the level of the intrusion:

$$\frac{d}{dz}(Q\bar{C}) = 2\pi\bar{b}(\alpha\bar{w})C_e, \quad z \leqslant z_i, \tag{10}$$

in which $\alpha\bar{w}$ is the horizontal entrainment velocity and $C_e(z)$ is the concentration of descending particles that are entrained into the plume calculated by following particle trajectories, as discussed in Sec. III C. In particular, the particle concentration at the height of the intrusion is $C_i \equiv \bar{C}(z_i)$.

For the following calculation of the radially spreading intrusions, we need to know the radial volume flux of intruding fluid, Q_i. This is set by the thickness, h_i, of the intrusion at the radius b_i where the intrusion becomes distinct from the plume.

The intrusion thickness at b_i is assumed to depend upon the distance between the intrusion height at the maximum height of the fountain according to

$$h_i = \gamma_h (Z_{\max} - z_i). \tag{11}$$

The intrusion being centered about z_i and its upper flank being no higher than $Z_{\max}$ means that γ_h should be no larger than 2.

The top-hat plume model assumes a discrete jump between the properties within and outside the plume. In reality it varies smoothly. So the radial distance from the plume beyond which particles are not influenced by re-entraining eddies is not necessarily the same as the top-hat plume radius b_{pi}. And so we introduce the parameter γ_b, which gives the distance

$$b_i = \gamma_b b_{pi}, \tag{12}$$

beyond which particles can fall from the intrusion free from the influence of eddies in the plume. The value of γ_b should be greater than unity.

With the estimates for h_i and b_i in Eqs. (11) and (12), respectively, the volume flux into intrusion is given by

$$Q_i = Q_{pi} b_{pi}^2 / (2 b_i h_i). \tag{13}$$

B. Radially spreading intrusions

Carey *et al.* [6,15] predicted the concentration of particles carried by a particle-bearing plume in a uniform-density ambient that impacts upon and spreads along a rigid horizontal surface. Their model neglected entrainment into the intrusion, assuming that the radial volume flux is constant. This assumption is reasonable for laboratory-scale experiments in which turbulent eddies were not apparent on the flanks of the intrusion. But it is questionably reliable for large-Reynolds-number flows typical of radially spreading volcanic eruptions. The transport of particles in the radially spreading flow, including their loss as they settle out of the intrusion at speed w_s, is given by

$$\frac{1}{r} \frac{\partial}{\partial r} (ruhC) = -w_s C, \tag{14}$$

in which u and h, respectively, are the outward radial flow speed and the height of the flow, and it is assumed that the concentration is uniform over the vertical extent of the intrusion. Assuming the radial flux of volume $Q_i = 2\pi ruh$ is constant along the flow, (14) can be solved to find the concentration in the region outside the plume:

$$C(r) = C_i \exp \left[-\frac{2\pi w_s}{Q_i} \left(r^2 - b_i^2 \right) \right], \quad r > b_i. \tag{15}$$

Note that the result does not explicitly depend upon the flow speed and depth of the intrusion. The intrusion thickness may be less than h_i for $r > b_i$. But the combination ruh is constant.

C. Particle settling

Finally we consider the path taken by particles as they fall back to the ground. In doing so, we suppose the vertical speed is set by the settling velocity and the radial speed is set by the process of ambient entrainment into the plume. Explicitly,

$$\frac{dr_p}{dt} = -u_a, \quad \frac{dz_p}{dt} = -w_s, \tag{16}$$

in which $u_a(r_p, z_p) = u_e(z_p)\bar{b}(z_p)/r_p$ for $r_p > \bar{b}(z_p)$, and, according to the entrainment assumption, $u_e = \alpha \bar{w}$.

Using the profile of $\bar{w} = M/Q$, computed numerically in assessing the upward propagation of the plume, (16) is integrated for a particle starting at $z_p = z_i$ and at $r_p = r$, for some $r > b_i$. The
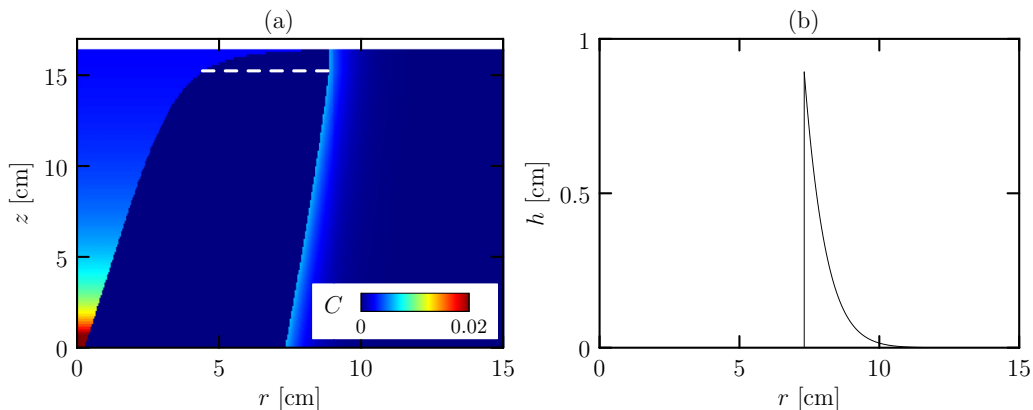
FIG. 6. (a) Concentration field in g/cm^3 as a function of radius and height computed from the numerical model and (b) predicted height of sedimented particles. Input parameters used for this computation are the same as those for experiment 10 (see Table I). In panel (a) the dashed white lines are drawn at the spreading height, z_i, and extend from the plume radius to where particles first rain out of the intrusion.

integration proceeds until $r_p \leqslant \bar{b}(z_p)$ (the particle is drawn into the plume) or $z_p \leqslant z_0$ (the height of the source), whichever occurs first. The process is repeated for a range of initial radii r between b_i and an outer radius much larger than $(Q_i/2\pi w_s)^{1/2}$.

We record the range of r from b_i to r_e for which particles are re-entrained into the plume. For $r > r_e$ we record the radius R at the time when $z_p = z_0$. This is where the particle finally settles to form a sediment bed about the source. Explicitly, the concentration about the source is given by (15) with r replaced by $R(r)$.

The combined results of the plume, intrusion, and settling calculations are illustrated by the particle concentration field shown in Fig. 6(a). This was computed using the input parameters from experiment 10 and using scaling parameters $\gamma_z = 0.9$, $\gamma_h = 1.0$, and $\gamma_b = 2.0$. In this case the neutral and maximum height of the plume are $Z_{\text{neutral}} = 3.50$ cm and $Z_{\text{max}} = 16.6$ cm, respectively, and the intrusion spreads at height $z_i = Z_{\text{neutral}} + \gamma_z(Z_{\text{max}} - Z_{\text{neutral}}) = 15.2$ cm. The plume radius at z_i is $b_{zi} = 4.42$ cm, and so the particles begin to rain out of the intrusion at $b_i = \gamma_b b_{zi} = 8.83$ cm. The intrusion thickness is $h_i = \gamma_h(Z_{\text{max}} - z_i) = 1.4$ cm.

The result shows that the concentration of particles drops significantly within the rising plume from a value $C_0 = 0.0295$ g/cm^3 at the source to $C_{zi} = 0.00258$ g/cm^3 at z_i. The decrease is directly related to the increase of volume flux from $Q_0 = 19.2$ cm^3/s to $Q_{zi} = 219$ cm^3/s, guaranteeing that the mass per time across the plume at any height remains fixed at $dm_0/dt = 0.567$ g/s. Likewise, the concentration, C_i, of particles at the radius b_i where they begin to rain out is set by ensuring that the mass per time entering the intrusion equals dm_0/dt. Hence $C_i = 0.00610$ g/cm^3.

As the particles settle from the intrusion, they are drawn toward the plume as a result of the radial flows induced by entrainment of fluid into the plume. In this particular computation all the particles reach the ground without being re-entrained into the plume.

D. Sediment depth

The three-step procedure above provides a numerical method through which, given source and ambient parameters Q_0, M_0, F_0, C_0, w_s, and N, the concentration, $C(R)$, of particles settling through z_0 can be calculated. The computation of sediment depth allows for the pile-up of particles over time while the plume is active. Departures from the steady-state prediction due to the starting and terminating plume are neglected under the assumption that the plume is in steady state much longer than the initial and final transient times [1,11].

If the plume is active for a total time T, the mass of sedimented particles per unit horizontal area is [6]

$$T Q_i \frac{1}{2\pi R} \frac{dC(R)}{dR}.$$

The corresponding height of the mound including interstitial fluid within the mound is

$$h(R) = \beta T Q_i \frac{1}{\rho_p} \frac{1}{2\pi R} \frac{dC(R)}{dR}, \tag{17}$$

in which ρ_p is the particle density. For a dense packing of spheres, $\beta = 3\sqrt{2}/\pi \simeq 1.35$. In our model we assumed a moderately less tight packing by setting $\beta = 1.5$.

As an example, the sediment depth as a function of radius computed using the parameters of experiment 10 is plotted in Fig. 6(b). When descending from the intrusion the concentration of particles as a function of radius had standard deviation of 2.71 cm with peak at radius $b_i = 6.19$ cm. While approaching the ground, the differential radial speed with radius means that the initial Gaussian distribution is distorted and the peak shifts closer to the plume. At the ground, the peak is situated at $r = 7.32$ cm and the standard deviation of the distribution to the right is $\sigma_h^\star = 0.93$ cm. The maximum height of the mound is 0.89 cm.

E. Particle recycling

If the modelled particles have smaller diameter so that the Stokes settling speed is smaller, a fraction of them can be drawn into the plume before reaching the ground. An example of this circumstance, computed using the input parameters of experiment 2 (the experiment shown in Fig. 2) is shown in Fig. 7(a). As above, the scaling parameters were $\gamma_z = 0.9$, $\gamma_h = 1.0$, and $\gamma_b = 2.0$. In this case, because $F_0 < 0$ the neutral height is taken to be $Z_{\text{neutral}} = 0$ cm. The maximum height of the plume is $Z_{\text{max}} = 10.5$ cm. The intrusion spreads at height $z_i = 9.5$ cm where the plume radius is $b_{zi} = 2.8$ cm, and the particles rain out for $r \geqslant b_i = 5.7$ cm. The mass per time leaving the intrusion is $dm_0/dt = 0.51$ g/s, equal to the mass per time emanating from the plume source. However, only 0.21 g/s reaches the ground while 0.30 g/s is re-entrained into the plume.

As a consequence of this re-entrainment, the evolution of the plume itself should change as a consequence of modification to the buoyancy flux according to (8) in which the ambient stratification (expressed through the buoyancy frequency, N) must now include the vertical density gradient due to particles as well as salinity at the edge of the plume. We set up an iterative procedure to account for this process of particle recycling [10,15].

With the known ambient particle concentration along the edge of the plume computed in the first iteration, we recompute N and use this to solve the plume equations (6)–(8). With this solution we determine the new intrusion level and the concentration of particles in the intrusion, and then the downward and inward radial motion of the particles is tracked. This gives a new distribution of particles being entrained into the plume and a new distribution of settled particles. Because particles enter the plume from the side as well as from the source, the mass per time of particles entering and falling from the intrusion is larger. Likewise, the mass per time of particles settling on the ground is larger, but still less than the mass per time of particles emanating from the source.

The procedure of recalculating N, the plume evolution, and the falling particles is repeated until the mass per time of particles falling on the ground is approximately equal to the mass per time of particles emanating from the source. For the circumstance shown in Figs. 7(c) and 7(d), this took 10 iterations, at which point 0.74 g/s of particles are re-entrained into the plume, 1.25 g/s of particles enter and fall out of the intrusion, and 0.50 g/s of particles settle on the ground, close to the 0.51 g/s input at the source.
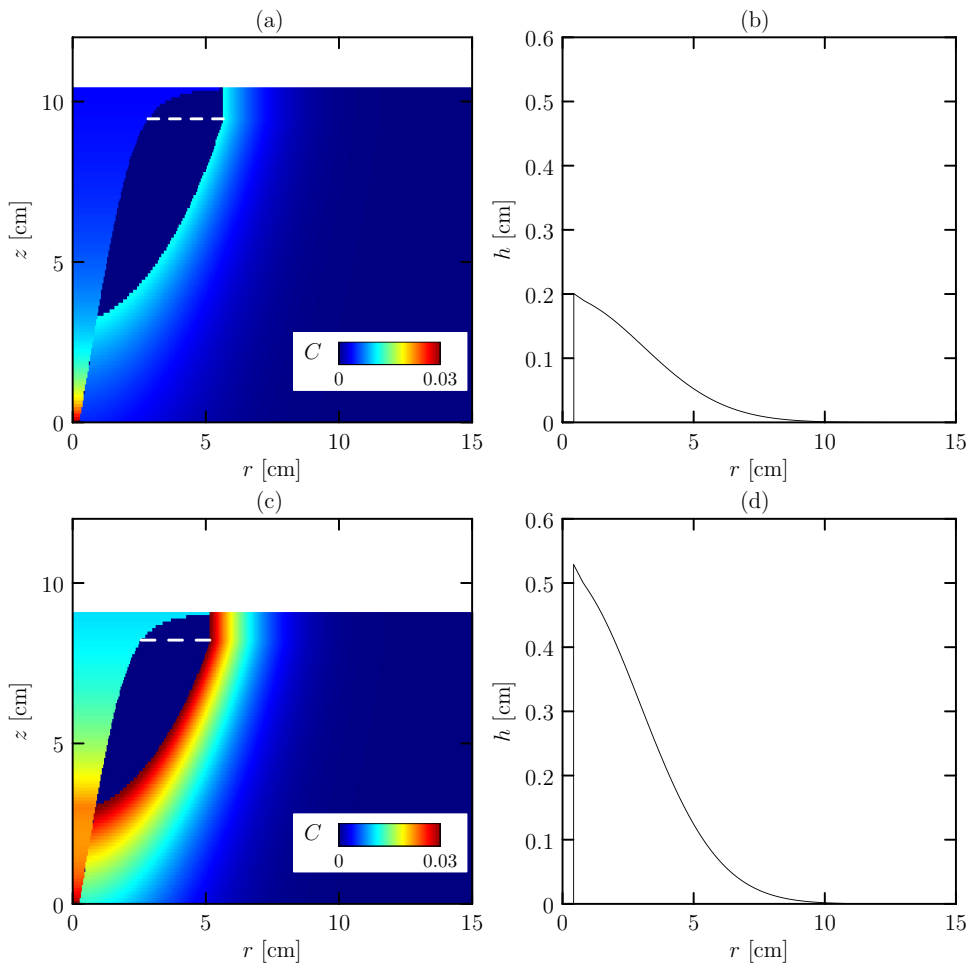
FIG. 7. Concentration field in g/cm³ as a function of radius and height computed from the numerical model (a) after the first iteration (not accounting for particle re-entrainment into the plume) showing (b) the corresponding particle mound height. (c) The concentration field computed after ten iterations and (d) its corresponding particle mound height. In each plot the dashed white lines are drawn at the spreading height, z_i, and extend from the plume radius to where particles first rain out of the intrusion.

F. Parameter sensitivity tests

The theoretical model has introduced three tunable parameters that influence particle transport and deposition. The value of γ_z, defined implicitly by (9), determines at what height the intrusion spreads radially from the plume. Lowering the value of γ_z significantly decreases the predicted maximum height of the sediment mound whereas the radial extent of the mound decreases only moderately. The value of γ_b, defined implicitly by (12), determines where the intrusion no longer interacts with the plume and particles begin to rain out. Increasing γ_b moderately decreases the radial extent of the sediment mound, though the dependence of the maximum height upon γ_b varies depending upon the degree of re-entrainment of falling particles back into the plume. The value of γ_h, defined implicitly by (11), determines the vertical extent of the intrusion at radius b_i and, together with b_i, determines the radial volume flux into the intrusion relative to the vertical volume flux within the plume at the intrusion height. Increasing γ_h moderately increases the maximum height of the sediment mound and moderately decreases its radial extent.

Through trial and error, best results for recycling particles were found by choosing $\gamma_z = 0.9$, $\gamma_b = 2.0$, and $\gamma_h = 1.0$.

IV. COMPARISON OF THEORY WITH EXPERIMENTS

Table I compares with experimental measurements the modelled intrusion height, $z_i^\star$, and the depth, $h_s^\star$, and width, $\sigma_s^\star$, of sedimented particles.

The comparison of intrusion heights between theory and experiments is reasonably good: The predicted intrusion height is within 20% of the observed spreading height in all but one experiment (experiment 8, for which the theory overpredicts the height by 22%). The error is acceptable, considering the error in the spreading height measurement is ± 2 cm. In experiments with the small particles ($d_p \simeq 100\,\mu$m), the predicted maximum settled-particle height is within 20% of observations for four experiments and is within 50% in all but one experiment (experiment 2, for which theory overpredicts the height by 56%). The predictions of the width of the settled particles are in poorer agreement. In the four small-particle experiments with $C_0 = 0.0295$ g/cm^3, the width is predicted to within 22% of observations. But the predictions are particularly poor for experiments with small concentrations, overpredicting the width by up to three times observations.

In the theory for experiments with large ($d_p \simeq 214\,\mu$m) particles, the settling velocity is so large that the particles do not re-entrain. Hence the particles are predicted to reach the ground at a large radius (7–8 cm) from the source. This distance depends sensitively upon the choice of γ_b, which sets the relative radius from the plume at which particles begin to rain out from the intrusion. In reality, the experiments showed that these large particles rapidly rained out of the intrusion and fell close to the plume. Far better agreement with observations is found if we set $\gamma_b = 1.0$ (in which case particle re-entrainment occurs) and $\gamma_h = 1.0$. For experiment 10, we find $h_s^\star = 0.49$ cm and $\sigma_s^\star = 3.98$ cm, respectively, within 4% and 65% of observed values. For experiment 11, $h_s^\star = 0.27$ cm and $\sigma_s^\star = 4.64$ cm, respectively, within 39% and 92% of observed values.

The need to adjust γ_b for experiments with relatively large particles is an indication that the treatment of the particles as passive within the plume and during the passage from plume to intrusion is poor when the settling speed becomes large relative to the mean upward speed of the plume at the height of the intrusion. Larger particles should settle within and close to the fountain where the magnitude of velocity fluctuations associated with eddies becomes comparable to the settling speed. These considerations should be less relevant for smaller particles that can be carried far from the plume before settling becomes significant.

Of course, the model assumes a steady-state solution and so neglects the fall of particles within the plume after the flow stops at the source. But this short-time transient cannot account entirely for the difference between the predicted and observed mound height and width. More likely are the many physical processes neglected in our model. We have neglected the complicated process of particle settling in the region between the rising plume, collapsing fountain, and radially spreading intrusion. We have also neglected the transport of ambient fluid in the wake of the particles as they fall, which influences their effective buoyancy and may also influence the ambient stratification through diffusive mixing between this trailing fluid and the ambient.

V. DISCUSSION AND CONCLUSIONS

We have performed experiments of particle-bearing plumes and fountains rising in uniformly stratified fluid, using a nonintrusive light-attenuation method to measure the structure of the settled particle mound after the end of the experiment. Generally we found the mound height as a function of radius was well represented by a Gaussian function with height h_s and standard deviation σ_s. The particle concentrations were no more than 4% by weight (1.5% by volume) and so we found that the height of intrusions emanating from the plume was consistent with previous observations and theory of particlefree plumes and fountains in stratified fluid [12,14,25,26].

To gain insight into the processes that affect the structure of the particle mound, we developed a model that combined plume theory [2] with an adaptation of the theory for the fall of particles from a radially spreading flow [6], and we included the effects of particle recycling [10]. Besides the plume entrainment parameter, $\alpha = 0.1$, and a parameter that determined the consolidation of particles in the mound, $\beta = 1.5$ (moderately greater than the value $\simeq 1.35$ for the dense packing of spheres), we introduced three new parameters: γ_z determined the intrusion height relative to the neutral buoyancy and maximum plume height; γ_b determined where downward settling from the intrusion dominated over the upward motion by eddies within the plume; and γ_h, which determined the intrusion thickness, a measure of the change in volume flux occurring in the fountain top. Best results were found by setting $\gamma_z = 0.9$, $\gamma_h = 1.0$, and $\gamma_b = 2.0$. Despite the simplifying assumptions of the theory, our results suggest the essential dynamics, particularly the influence of particle re-entrainment and recycling, were captured.

Because of the idealizations of the experiments and theory, it would be premature to extend these results to predict the spread of ash from Plinian volcanic explosions. In those systems, the column of ash rises through nonuniformly stratified fluid, the particles have wide-ranging sizes, and winds often render the flow nonaxisymmetric. But the comparison of theoretical with experimental results is encouraging in that the relatively simple model can capture the leading-order dynamics.

[1] A. W. Woods, Turbulent plumes in nature, Annu. Rev. Fluid Mech. **42**, 391 (2010).

[2] B. R. Morton, G. I. Taylor, and J. S. Turner, Turbulent gravitational convection from maintained and instantaneous sources, Proc. R. Soc. London, Ser. A **234**, 1 (1956).

[3] T. J. McDougall, Negatively buoyant vertical jets, Tellus **33**, 313 (1981).

[4] L. J. Bloomfield and R. C. Kerr, A theoretical model of a turbulent fountain, J. Fluid Mech. **424**, 197 (2000).

[5] G. G. Rooney and B. J. Devenish, Plume rise and spread in a linearly stratified environment, Geophys. Astrophys. Fluid Dyn. **108**, 168 (2014).

[6] R. S. J. Sparks, S. N. Carey, and H. Sigurdsson, Sedimentation from gravity currents generated by turbulent plumes, Sedimentology **38**, 839 (1991).

[7] P. G. Baines, M. T. Jones, and R. S. J. Sparks, The variation of large-magnitude volcanic ash cloud formation with source latitude, J. Geophys. Res. **113**, D21204 (2008).

[8] C. G. Johnson, A. J. Hogg, H. E. Huppert, R. S. J. Sparks, J. C. Phillips, A. C. Slim, and M. J. Woodhouse, Modelling intrusions through quiescent and moving ambients, J. Fluid Mech. **771**, 370 (2015).

[9] G. G. J. Ernst, R. S. J. Sparks, S. N. Carey, and M. I. Bursik, Sedimentation from turbulent jets and plumes, J. Geophys. Res. **101**, 5575 (1996).

[10] G. Veitch and A. W. Woods, Particle recycling and oscillations of volcanic eruption columns, J. Geophys. Res. **105**, 2829 (2000).

[11] A. W. Woods and C. P. Caulfield, A laboratory study of explosive volcanic eruptions, J. Geophys. Res. **97**, 6699 (1992).

[12] L. J. Bloomfield and R. C. Kerr, Turbulent fountains in a stratified fluid, J. Fluid Mech. **358**, 335 (1998).

[13] J. K. Ansong and B. R. Sutherland, Internal gravity waves generated by convective plumes, J. Fluid Mech. **648**, 405 (2010).

[14] T. S. Richards, Q. Aubourg, and B. R. Sutherland, Radial intrusions from turbulent plumes in uniform stratification, Phys. Fluids **26**, 036602 (2014).

[15] S. N. Carey, H. Sigurdsson, and R. S. J. Sparks, Experimental studies of particle-laden plumes, J. Geophys. Res. **93**, 15314 (1988).

[16] H. N. Mirajkar, S. Tirodkar, and S. Balasubramanian, Experimental study on growth and spread of dispersed particle-laden plume in a linearly stratified environment, Environ. Fluid Mech. **15**, 1241 (2015).

[17] R. J. Munro and S. B. Dalziel, Attenuation technique for measuring sediment displacement levels, Expt. Fluids **39**, 600 (2005).

[18] R. J. Munro, N. Bethke, and S. B. Dalziel, Sediment resuspension and erosion by vortex rings, Phys. Fluids **21**, 046601 (2009).

[19] B. R. Sutherland and S. B. Dalziel, Bedload transport by a vertical jet impinging upon sediments, Phys. Fluids **26**, 035103 (2014).

[20] L. Wilson, R. S. J. Sparks, T. C. Huang, and N. D. Watkins, The control of volcanic column heights by eruption energetics and dynamics, J. Geophys. Res. **83**, 1829 (1978).

[21] R. E. Holasek, A. W. Woods, and S. Self, Experiments on gas-ash separation processes in volcanic umbrella plumes, J. Volcanol. Geotherm. Res. **70**, 169 (1996).

[22] G. Carazzo and A. M. Jellinek, A new view of the dynamics, stability and longevity of volcanic clouds, Earth Planet. Sci. Lett. **325**, 39 (2012).

[23] G. Carazzo and A. M. Jellinek, Particle sedimentation and diffusive convection in volcanic ash clouds, J. Geophys. Res. **118**, 1420 (2013).

[24] G. Oster, Density gradients, Sci. Am. **213**, 70 (1965).

[25] C. P. Caulfield and A. W. Woods, Plumes with non-monotonic mixing behaviour, Geophys. Astrophys. Fluid Dyn. **79**, 173 (1995).

[26] E. J. List, Turbulent jets and plumes, in *Mixing in Inland and Coastal Waters*, edited by H. B. Fischer, E. J List, R. C. Y. Koh, J. Imberger, and N. H. Brooks (Academic Press, San Diego, 1979), pp. 315–389.

[27] C. Bonadonna and J. C. Phillips, Sedimentation from strong volcanic plumes, J. Geophys. Res. **108**, 2340 (2003).

[28] A. Costa, G. Macedonio, and A. Folch, A three-dimensional Eulerian model for transport and deposition of volcanic ashes, Earth Planet. Sci. Lett. **241**, 634 (2006).

[29] A. Costa, A. Folch, and G. Macedonio, A model for wet aggregation of ash particles in volcanic plumes and clouds, 1: Theoretical formulation, J. Geophys. Res. **115**, B09201 (2010).

[30] R. M. Dorrell, A. J. Hogg, E. J. Sumner, and P. J. Talling, The structure of the deposit produced by sedimentation of polydisperse suspensions, J. Geophys. Res. **116**, F01024 (2011).

[31] G. Carazzo, E. Kaminski, and S. Tait, The route to self-similarity in turbulent jets and plumes, J. Fluid Mech. **547**, 137 (2006).

[32] M. van Reeuwijk and J. Craske, Energy-consistent entrainment relations for jets and plumes, J. Fluid Mech. **782**, 333 (2015).